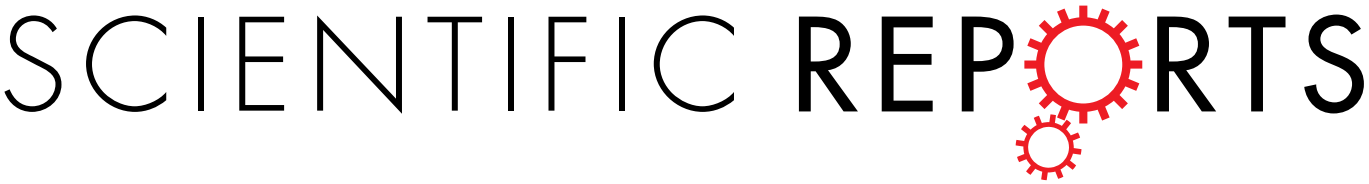

OPEN

UV Degradation and Recovery of Perovskite Solar Cells

Sang-Won Lee[1], Seongtak Kim[1], Soohyun Bae[1], Kyungjin Cho[1], Taewon Chung[1], Laura E. Mundt[2], Seunghun Lee[1,2], Sungeun Park[1,2], Hyomin Park[1], Martin C. Schubert[2], Stefan W. Glunz[2,3], Yohan Ko[4], Yongseok Jun[4], Yoonmook Kang[5], Hae-Seok Lee[5] & Donghwan Kim[1]

Received: 10 August 2016
Accepted: 01 November 2016
Published: 02 December 2016

Although the power conversion efficiency of perovskite solar cells has increased from 3.81% to 22.1% in just 7 years, they still suffer from stability issues, as they degrade upon exposure to moisture, UV light, heat, and bias voltage. We herein examined the degradation of perovskite solar cells in the presence of UV light alone. The cells were exposed to 365 nm UV light for over 1,000 h under inert gas at <0.5 ppm humidity without encapsulation. 1-sun illumination after UV degradation resulted in recovery of the fill factor and power conversion efficiency. Furthermore, during exposure to consecutive UV light, the diminished short circuit current density (J_{sc}) and EQE continuously restored. 1-sun light soaking induced recovery is considered to be caused by resolving of stacked charges and defect state neutralization. The J_{sc} and EQE bounce-back phenomenon is attributed to the beneficial effects of PbI_2 which is generated by the decomposition of perovskite material.

Power conversion efficiency (PCE) of orreganic-inorganic hybrid perovskite solar cells has increased from 3.81% to 22.1% in just 7 years[1,2]. In 2009, Kojima *et al.* reported the first application of $CH_3NH_3PbI_3$ and $CH_3NH_3PbBr_3$ perovskites as sensitizers for photovoltaic devices[1]. Perovskite absorbers have an ABX_3 crystal structure[3–5], usually composed of an organic material (A site), a metal (B site), and a halide (X site). The A site is usually occupied by methylammonium (CH_3NH_3), formamidinium ($HC(NH_2)_2$), or a combination of both materials. Recently, the addition of cesium (Cs) and guanidinium (Gu) has been reported[6–9]. Generally, the B site is occupied by metals (e.g., lead (Pb) or tin (Sn)), while the X site is occupied by halides such as iodine (I), bromine (Br), or chlorine (Cl). This organic-inorganic hybrid material has a number of beneficial characteristics that render it suitable for photovoltaic applications. For example, a high absorption coefficient (~10^5 cm^{-1})[10–14], long diffusion length (~1 μm)[15,16], direct band gap, and multiple fabrication methods[15,17–19]. Development of all solid-state perovskite solar cells containing Spiro-MeOTAD, optimization of the fabrication processes, device structures, and material substitution/addition have been investigated to obtain higher PCE[10,17–21]. In addition, because of the tunable band-gap[22,23] and simple fabrication steps, perovskite solar cells are an attractive candidate for tandem applications, enabling >30% efficiency potential[24–27].

Despite such attractive properties, a number of challenges prevent the commercialization of perovskite solar cells, such as the lack of stability, use of Pb, and scale-up issues. Although the replacement of Pb with Sn or other materials is of particular interest, Sn-based perovskite solar cells show even lower stability than Pb-based perovskite congeners[28–30]. Issues regarding scale-up have been addressed by the development of evaporation[19], doctor blade[31], roll-to-roll[32], and inkjet printing[33] processes; however, stability problems still need to be solved. According to previous literature reports, the stability of perovskite solar cells is influenced by four main factors: moisture[34–36], heat[37,38], voltage[39], and UV light[34,40], with moisture being the most critical factor. Attempts to improve the stability of perovskite solar cells have focused on encapsulation[40,41], replacement/substitution of selective contacts[42,43], interlayer insertion[44,45], development of novel cell and module configurations[46,47], and modification of the perovskite light-absorbing material[6,23,42,48–50]. Nevertheless, issues relating to stability have still not been resolved, and therefore, further studies must be carried out.

[1]Korea University, Department of Materials Science and Engineering, Seoul, 136-713, Republic of Korea. [2]Fraunhofer Institute for Solar Energy Systems ISE, Freiburg, 79110, Germany. [3]University Freiburg, Laboratory for Photovoltaic Energy Conversion, Freiburg, 79110, Germany. [4]Konkuk University, Department of Materials Chemistry and Engineering, Seoul, 143-701, Republic of Korea. [5]KU·KIST Green School, Graduate School of Energy and Environment, Korea University, Seoul, 136-713, Republic of Korea. Correspondence and requests for materials should be addressed to Y.K. (email: ddang@korea.ac.kr) or H.-S.L. (email: lhseok@korea.ac.kr) or D.K. (email: solar@korea.ac.kr)

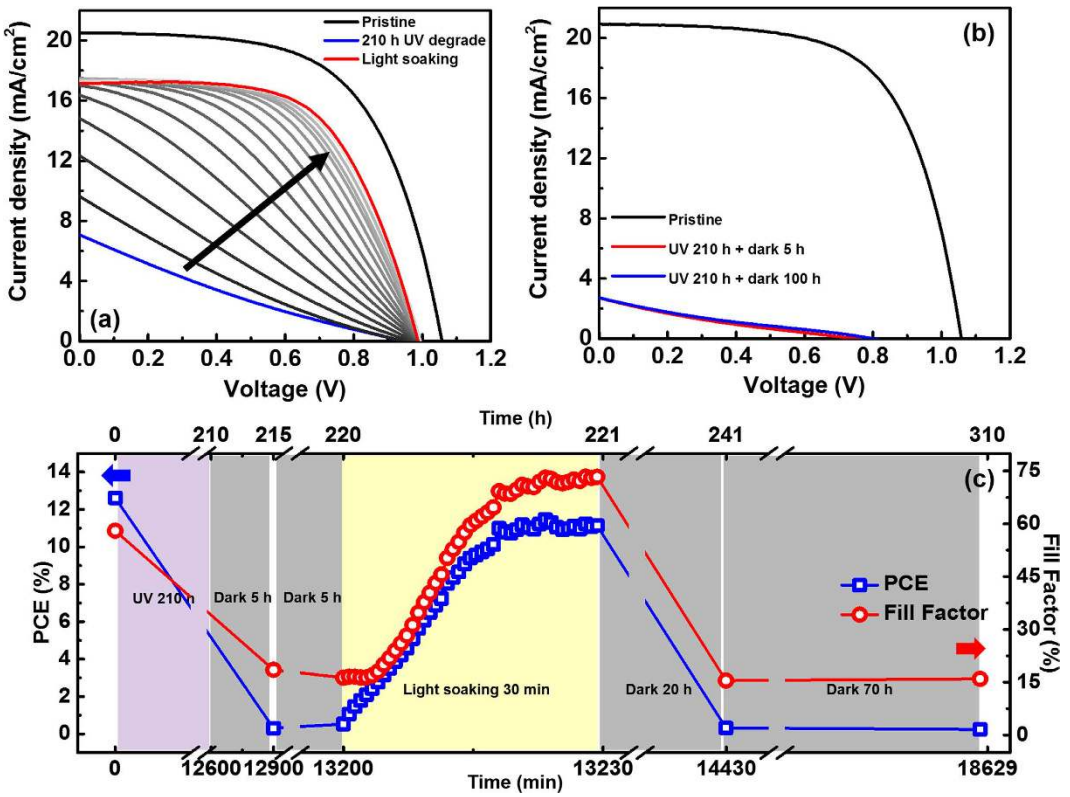

Figure 1. Light-IV curve of (**a**) a pristine device, 210 h UV exposed, during 15 min light soaking and (**b**) pristine device, 210 h UV exposed and then rested in dark under inert gas atmosphere for 5 h and 100 h. (**c**) PCE and FF of a device with denoted light conditions.

In particular, stability upon UV light exposure (hereafter, UV stability), the photocatalytic effect of TiO_2 is discussed as a main reason of perovskite degradation. Niu *et al.* reported that perovskite underwent degradation upon UV irradiation in the presence of both moisture and oxygen[34]. Snaith *et al.* then reported enhanced UV stability with UV filter or upon substitution of TiO_2 with Al_2O_3[40]. In addition, Ito *et al.* identified the interface between the perovskite and the mesoporous TiO_2 scaffold as the area of cell degradation commencing, reporting enhanced stability with the incorporation of an Sb_2S_3 interlayer at the TiO_2/perovskite interface[45]. All of these studies have been conducted to under moisture- and oxygen-containing atmosphere with AM1.5G (1-sun) full solar spectrum irradiation. However, under such conditions, determination of the effects of UV light alone on perovskite degradation is challenging, since all wavelengths of light are employed and perovskite solar cells are particularly sensitive to moisture.

Herein, to investigate the effects of UV light alone on the degradation of perovskite solar cells, UV stability experiments were conducted in a glove box (<0.5 ppm average humidity, Ar atmosphere, 25 °C), wherein perovskite solar cells were exposed to 365 nm UV light over the course of 1,000 h under open circuit condition. The power of the UV light employed in this study was approximately 7.6 mW·cm^{-2}, giving a UV intensity approximately 1.5 times higher than that in the AM1.5G 100 mW·cm^{-2} solar spectrum, which has a UV intensity of only 4.6 mW·cm^{-2} at wavelengths below 400 nm[44]. Continuous degradation of perovskite solar cell performance was observed even in the absence of moisture, oxygen, and longer wavelength light. Interestingly, UV-degraded FF and PCE of the perovskite solar cell were recovered upon subsequent 1-sun illumination. In case of the J_{sc} and EQE, rapidly decreased values bounced back continuously with consecutive UV light exposure. The processes involved in UV degradation and recovery of the perovskite solar cells were characterized by UV-visible spectroscopy, X-ray diffraction (XRD), light current-voltage (LI-V), external quantum efficiency (EQE), Electrochemical Impedance Spectroscopy (EIS), μ-photoluminescence spectroscopy (μ-PLS), and μ-light beam induced current (μ-LBIC) analyses.

Results

UV degradation under inert gas and beneficial effect of degradation by-product PbI_2. Figure 1a shows LI-V curves of 210 h UV exposed perovskite solar cell under inert gas atmosphere at open circuit and 1-sun light soaking result. Although UV light was exposed under inert gas atmosphere, UV exposure made significant degradation on perovskite solar cells. However, UV degradation was recovered by 1-sun light soaking. Initially 12.2% efficiency was degraded to 1.36% during UV exposure and recovered to 10.4% with continuous 1-sun light soaking. During recovery process, there was no significant change in XRD peaks (Supplementary Fig. S1). On the other hand, UV degradation was not recovered when device rested in dark as shown in Fig. 1b. 1-sun light soaking induced recovery was also occurred after 10 h delay in dark. Figure 1c shows PCE and FF values when

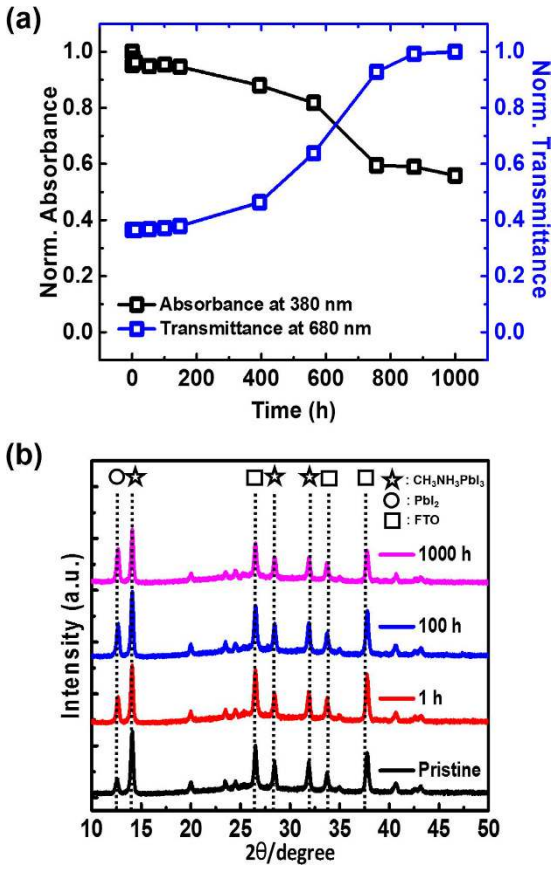

Figure 2. (**a**) Normalized light absorbance (at 380 nm) and transmittance (at 680 nm). (**b**) X-ray diffraction patterns of the devices following UV exposure.

devices exposed to UV light, 1-sun light, and rested in dark. When device was rested in dark after 1-sun light soaking recovery, device performance was retrogressed to degraded state. The J_{sc} and open circuit voltage (V_{oc}) show similar tendency (Supplementary Fig. S2a,b). To investigate detail steps of UV degradation and recovery, new set of devices was exposed to UV light during 1,000 h and characterized at specific times. Figure 2 shows the normalized light absorbance and X-ray diffraction patterns of UV exposed perovskite devices for different times.

During UV exposure under Ar atmosphere, the light absorption of the perovskite device started to decrease after 200 h, accompanied by increase in transmittance. This can be understood as perovskite materials started to lose their ability to absorb light after 200 h UV exposure. Full absorbance and transmittance data are presented in Supplementary Fig. S3. The X-ray diffraction patterns presented in Fig. 2b show several strong peaks, where the peaks at 14.1°, 28.5°, and 31.9° can be assigned to the (110), (220), and (310) planes of the $CH_3NH_3PbI_3$ perovskite. 12.6° peak corresponded to traces of PbI_2 that remained during device fabrication, which is in agreement with the results of previous studies[51]. The remaining peaks corresponded to the FTO substrate[21,44,51]. With increasing UV exposure time, the ratio between the PbI_2 (12.6°) and $CH_3NH_3PbI_3$ (14.1°) peaks increased and this means $CH_3NH_3PbI_3$ perovskite decomposing to PbI_2 continuously[34,44,45].

Figure 3 and Table 1 show multiple light I-V measurements acquired during 1,000 h UV exposure under open circuit conditions. The parameters, summarized in Fig. 3 and Table 1, are the fully recovered values with 1-sun light soaking as indicated in Fig. 1. In Fig. 3a,b, UV degradation began immediately after 1 h of UV exposure and significant degradation occurred at 100 h. From 100–200 h, PCE degradation retarded because of the increasing J_{sc}. 200–1,000 h, there was a continuous degradation in device performance with a decrease in V_{oc}, J_{sc}, and FF. Exposure to UV for 1,000 h led to 65% degradation of the PCE, while the FF exhibited the most pronounced degradation during this period. As shown in Fig. 3c, V_{oc} underwent little degradation before 400 h, except for the initial degradation. But V_{oc} subsequently dropped to 0.8 V during 400–1,000 h. Figure 3e shows an unexpected behaviour of the J_{sc}. Initial 20 h of the exposure made sharp fell of J_{sc}. However, after rapid degradation, current bounce back reaching almost 90% of the initial value was observed. This phenomenon can be accounted for beneficial effects of the degradation by-product PbI_2. The beneficial effect of PbI_2 on perovskite solar cells has been described in recent literatures[51–56.] Supasai *et al.* reported the passivation effect of PbI_2 and reduced defect states following PbI_2 generation[54]. In addition, Chen *et al.* reported that PbI_2 can passivate recombination sites at both the perovskite grain boundary and the perovskite/TiO_2 interface, thus improving the electrical properties of the device[52]. Also Kim *et al.* reported greatly improved solar cell performance and reduced hysteresis in the presence of PbI_2[53].

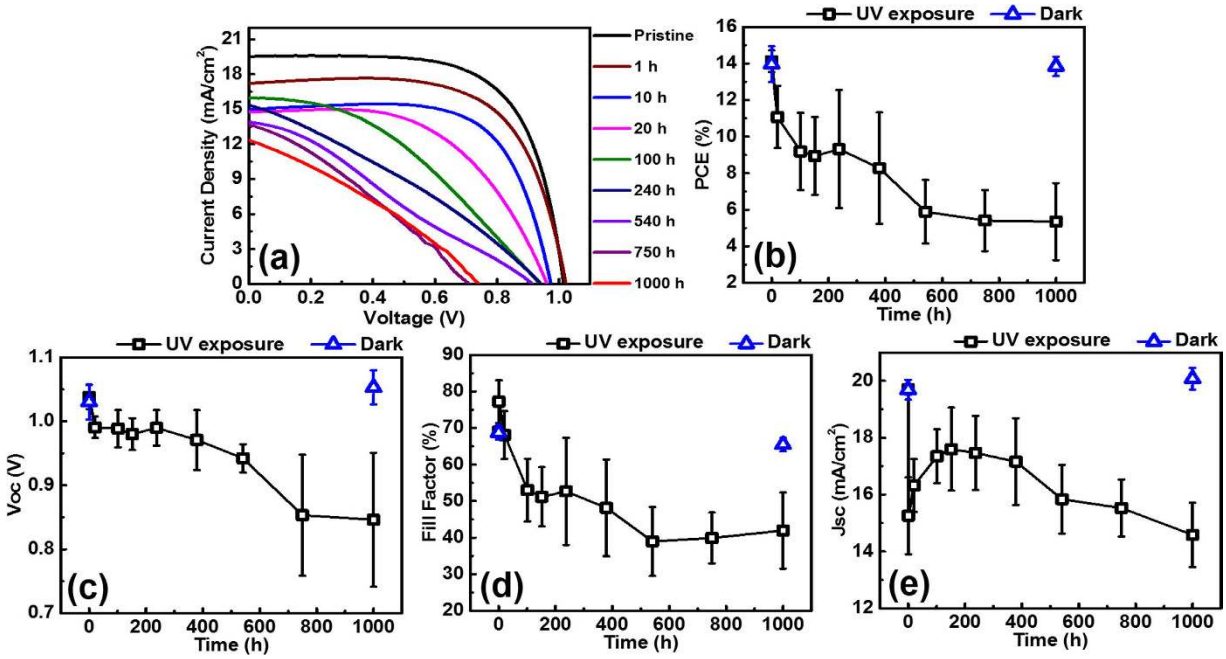

Figure 3. (**a**) Light I-V curve following the denoted UV exposure times. Variation in (**b**) PCE, (**c**) V_{oc}, (**d**) FF, and (**e**) J_{sc} with increasing UV exposure time (error bars are shown). All values are average obtained for six cells. The blue triangular symbol denotes the measurement for another device stored in the dark for 1,000 h. Perovskite solar cells were tested at the indicated UV exposure times. IV-measurement was conducted under AM1.5G 100 mW·cm^{-2} illumination. The voltage time setting was 200 ms, the active area was 0.125 cm^2, and a 0.075 cm^2 mask was used. Measurements were carried out in the open circuit voltage to short circuit voltage direction (i.e., reverse direction). For the measurement, devices were removed from the glove box and characterization was conducted under air at room temperature. A relative humidity of approximately 25% was maintained. During measurement, there was continuous increase in solar cell parameters as discussed later. Here, saturated values are presented.

UV Exposure Time [hour]	V_{oc} [V]	J_{sc} [mA·cm^{-2}]	FF [%]	PCE [%]
Pristine	1.038 (1.03 Stored in Dark)	19.71 (19.69 Stored in Dark)	69.02 (68.78 Stored in Dark)	14.12 (13.97 Stored in Dark)
1	0.992	15.26	77.21	11.64
13	0.986	15.87	70.39	11.03
21	0.991	16.32	68.08	11.07
102	0.988	17.35	53.00	9.19
152	0.980	17.60	51.16	8.94
237	0.990	17.47	52.67	9.32
379	0.971	17.16	48.14	8.28
541	0.942	15.83	38.96	5.89
750	0.853	15.53	39.90	5.41
1000	0.846 (1.053 Stored in Dark)	14.58 (20.08 Stored in Dark)	41.94 (65.47 Stored in Dark)	5.35 (13.84 Stored in Dark)

Table 1. Solar cell parameters during UV exposure (all values are an average of data obtained from six cells).

Consequently, UV degradation and recovery process can be explained by generation of traps (defects, charge stack) and simultaneous passivation and neutralization of these traps by PbI_2, which is generated as degradation by-product of perovskite. Initial 10 h UV exposure will produce abundant traps. These traps bring rapid fell of all solar cell parameters as shown in Fig. 3. However, in 10–200 h, as UV light degradation progress, PbI_2 would be generated. This PbI_2 will continuously passivate existing traps and enhance electron extraction. As a result of traps passivation, the V_{oc} slightly increased with retarded degradation. Also, enhanced electron extraction will produce the J_{sc} bounce back. Meanwhile, the FF continuously decreased because PbI_2 is not conductive materials. As UV degradation progressed further, much more PbI_2 will be generated and after a certain point, the cell parameters decreased again, as shown in Fig. 3 200–1,000 h. Improved electron extraction with PbI_2 passivation is verified by EIS measurement and possible energy band structure change is shown in Supplementary Fig. S4. Increased recombination resistance observed with 200 h UV exposure times.

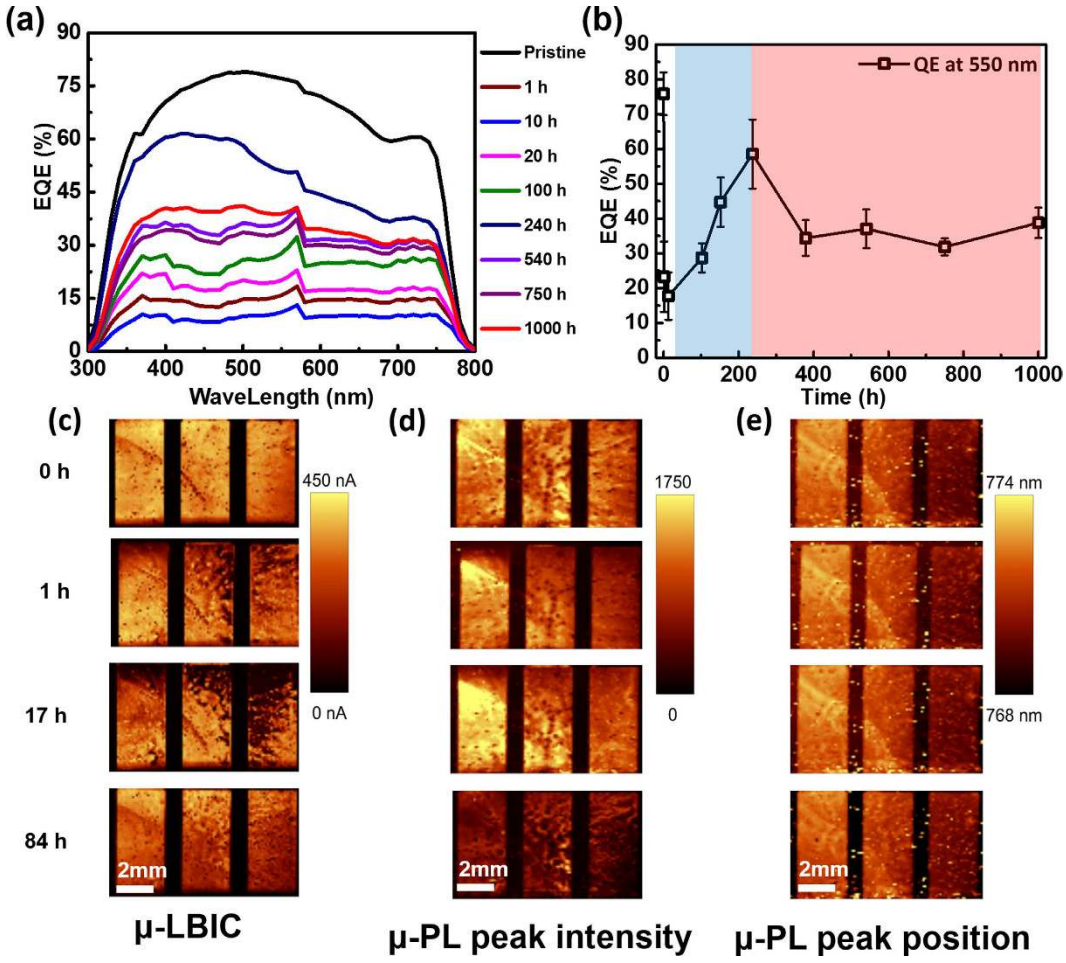

Figure 4. (**a**) EQE at 300–800 nm, and (**b**) at 550 nm for devices subjected to UV exposure for times in the range 0–1,000 h. Results are an average of data for six samples. Spatially resolved results: (**c**) μ-LBIC, (**d**) μ-PL peak intensity in arbitrary units, and (**e**) peak position in nm. Three single cells, which are located on one glass substrate, are depicted (ea. 0.125 cm^2). The cells were illuminated from the glass side using a 640 nm laser.

Current bounce back during UV degradation. The J_{sc} bounce back phenomenon was also found in EQE measurements. Figure 4a shows the variation in the EQE of the perovskite solar cells upon exposure to UV light. The EQE followed a similar tendency to that previously described for a J_{sc} (Fig. 3e), with almost 70% of the initial loss being recovered. This can be more clearly observed in Fig. 4b, which shows the variation in the EQE at 550 nm.

At the first period of UV degradation, the J_{sc} and EQE decreased rapidly. Initial rapid decrease is not directly due to $CH_3NH_3PbI_3$ decomposition. As shown in Fig. 2a,b, light absorbance and $CH_3NH_3PbI_3$ (peak at 14.1°) shows almost no change during the first period of UV degradation. This is more likely to be due to the changes of interfaces in the perovskite device like trap formation. Traps at interfaces may block electron extraction by capturing carriers and induce lowered current. In the second period (20–250 h), the J_{sc} and EQE underwent a bounce back. This can be attributed to the beneficial effects of the degradation by-product PbI_2. As mentioned previously, the generated PbI_2 can passivate recombination sites and improve the carrier extraction[51–55]. In the third period (250–1,000 h), the J_{sc} and EQE decreased once again due to further degradation of $CH_3NH_3PbI_3$, with a resulting decrease in the perovskite light absorbance and device performance.

To gain insight into the current bounce-back phenomenon, spatially resolved μ-LBIC and μ-PLs measurements were obtained by analysing a new set of devices with Au electrodes. The μ-LBIC (Fig. 4c) data generally corroborate the EQE and I-V measurements, exhibiting both degradation and recovery within the 84 h. The peak intensity (Fig. 4d), which is a function of the carrier density, changed significantly during the investigation. It decreases considerably after 84 h, as indicated by dark (low PL intensity) regions on the entire device. In contrast to the peak intensity, analysis of the spectral position of the PL peak (Fig. 4e) indicates that the bandgap of the absorber material is not affected by UV exposure, as also confirmed by the absorbance and XRD data shown in Fig. 2. Based on the fact that PL intensity is either caused by radiative recombination, at least until 17 h UV exposure, $CH_3NH_3PbI_3$ perovskite was not degraded much. However, between 17–84 h, PL intensity decreased significantly and this means lower radiative recombination or higher non-radiative recombination (trap-assisted). This also confirm that initial degradation of perovskite device was not mainly because of $CH_3NH_3PbI_3$ material

degradation. Until now it is not clear how the interfaces influence the degradation/recovery mechanism as the used characterization methods yield no information about that at the moment, but this will be addressed in following work.

UV degradation and 1-sun light soaking induced recovery. As previously mentioned in Fig. 1, UV degradation/recovery was repeated throughout the investigation. Figure 5 and Supplementary Fig. S5 present UV degradation/recovery during 1,000 h and at specific time. Degradation/recovery phenomenon of perovskite solar cells was also observed for other devices (Supplementary Figs S6–10). Supplementary Fig. S11a shows I-V curves for the pristine, UV-degraded, and partly recovered devices. Parameters are summarized in Supplementary Table S1. With 1-sun light soaking, PCE, FF, V_{oc}, R_s and R_{shunt} (Figs S11b,c,d,f) underwent continuous recovery up to saturation. The J_{sc} (Supplementary Fig. S11d) exhibited a rapid increase in the first stage of 1-sun light soaking, followed by a continuous decrease.

Discussion

Repeated UV degradation and 1-sun light soaking induced recovery attribute to the interface and bulk trap neutralization by photo-generated carriers. As a results of trap neutralization, electron extraction will be enhanced and this will improve V_{oc}, R_s, R_{shunt} and overall FF[57–61] during 1-sun light soaking. Consequently, UV degradation/recovery cycle can be explained by repeated process of interface defects generation by UV light and neutralization by photo-generated carriers under 1-sun light soaking. During this cycle, the photocatalytic effect of the mesoporous TiO_2 layer causes decomposition of the $CH_3NH_3PbI_3$ perovskite to PbI_2; degradation tendency can be seen in Fig. 5 (red line, UV degradation) and Fig. 2 [40,44,45]. As shown is Supplementary Fig. S11d, rapid recovery and continuous degradation of the J_{sc} during 1-sun light soaking can be explained by light-induced meta-stable trap formation at the perovskite bulk during 1-sun illumination. According to the literature, continuous 1-sun illumination will generate a quasi-static charge state by lattice distortion and phase separation. These states will be accumulated and coexist with photo-generated carriers, leading to current degradation during further 1-sun light soaking[22,62–64].

When devices were exposed to UV light hundreds of hours, UV degradation/recovery mechanism seems to be changed. 650 h UV exposed devices were recovered with 1-sun light soaking and stored in the dark to more detail investigation. If recovery process is related to interface defects only, the system should return to its initial position because of the de-trapping of carriers as indicated in Fig. 1. Supplementary Fig. S12, shows very little change with storing in the dark (Ar atmosphere). This suggest longer UV exposure can change UV degradation/recovery mechanism. Light-induced meta-stable trap states[22,62,63] and holes accumulation[65] can have rules in UV degradation/recovery.

Meta-stable trap states and charges are expected to accumulate primarily on the TiO_2/perovskite interface. Supplementary Fig. S13a shows the UV-Vis transmittance profile of the perovskite device components in the UV region, in addition to the calculated relative UV light intensity inside of the perovskite device by the Lambert law of absorption. Based on the transmittance and absorption coefficients of $CH_3NH_3PbI_3$[10–14], Supplementary Fig. S13b gives the calculated UV light intensity decay. Based on the calculations shown in Supplementary Fig. S13b, we propose a possible mechanism for the UV degradation/recovery of the perovskite solar cells. As indicated in Fig. 6, because UV light cannot penetrate deep into the perovskite device, UV light will be absorbed close to the interface of perovskite/TiO_2. As a results, meta stable trap-states and charges accumulation occur close to the mesoporous TiO_2/perovskite interface. In this case, perovskite bulk has not enough electrons to change position with the holes allowing it to flow to the hole transport material (HTM) side. Such electron deficiency can result in trapped holes. The accumulated meta-stable trap states and charges will be generated in following UV irradiation. These traps and charges can extract electrons from the iodine anion (I^-) in the $CH_3NH_3PbI_3$ crystals. This will compromise the perovskite crystal structure, producing PbI_2. Furthermore, residual traps and charges can also capture free electrons generated upon subsequent 1-sun light irradiation and can block the current flow, resulting in a transiently lowered solar cell performance with a low FF. 1-sun light irradiation will generate free carriers in whole regions of the perovskite light absorber, and these carriers can neutralize accumulated trap states and charges, resulting in the recovered device performance.

In this paper, degradation of mesoscopic $CH_3NH_3PbI_3$ perovskite by UV light alone was evaluated. UV degradation occurred in the absence of moisture and other wavelengths of light, likely due to the photocatalytic effect of mesoporous TiO_2, accumulated interface trap states and charges. A current bounce-back phenomenon was attributed to the trap passivation and enhanced electron extraction by UV degradation by-product PbI_2. The UV-degraded cell performance was subsequently recovered by 1-sun light soaking, with $>$60% of the initial degradation being recovered, and this degradation/recovery cycle could be repeated. The mainly degraded/recovered parameter was the fill factor. UV degradation/recovery phenomenon was considered as the neutralization and resolving of accumulated traps states and charges by free carriers generated by 1-sun light soaking.

Methods

FTO glass substrates (7 Ω/sq) were rinsed with acetone, ethanol, and isopropyl alcohol (IPA) with sonication. The substrate was then subjected to UV ozone treatment for 30 min. A compact TiO_2 layer was spin-coated with a 0.15 M titanium diisopropoxide bis(acetylacetonate) solution (75 wt%, Sigma-Aldrich) in 1-butanol (ACS reagent, $\geq$99.4%, Sigma-Aldrich), and the resulting TiO_2 layer was heat-treated for 15 min at 500 °C. Subsequently, a mesoporous TiO_2 solution was prepared by mixing TiO_2 paste (18NR-T Transparent titania paste, Dyesol), terpineol (mixture of isomers, anhydrous, Sigma-Aldrich), and ethyl alcohol (pure, 200 proof, anhydrous, Sigma-Aldrich) in a 1:4:2 wt% ratio, followed by heat treatment at 550 °C for 60 min. The $CH_3NH_3PbI_3$ perovskite layer was then prepared according to a previously reported sequential deposition method[17]. Lead(II) iodide powder (PbI_2, 99.9985% metal basis, Alfa Aesar) was dispersed in *N*,*N*-dimethylformamide (DMF, anhydrous, 99.8%, Sigma

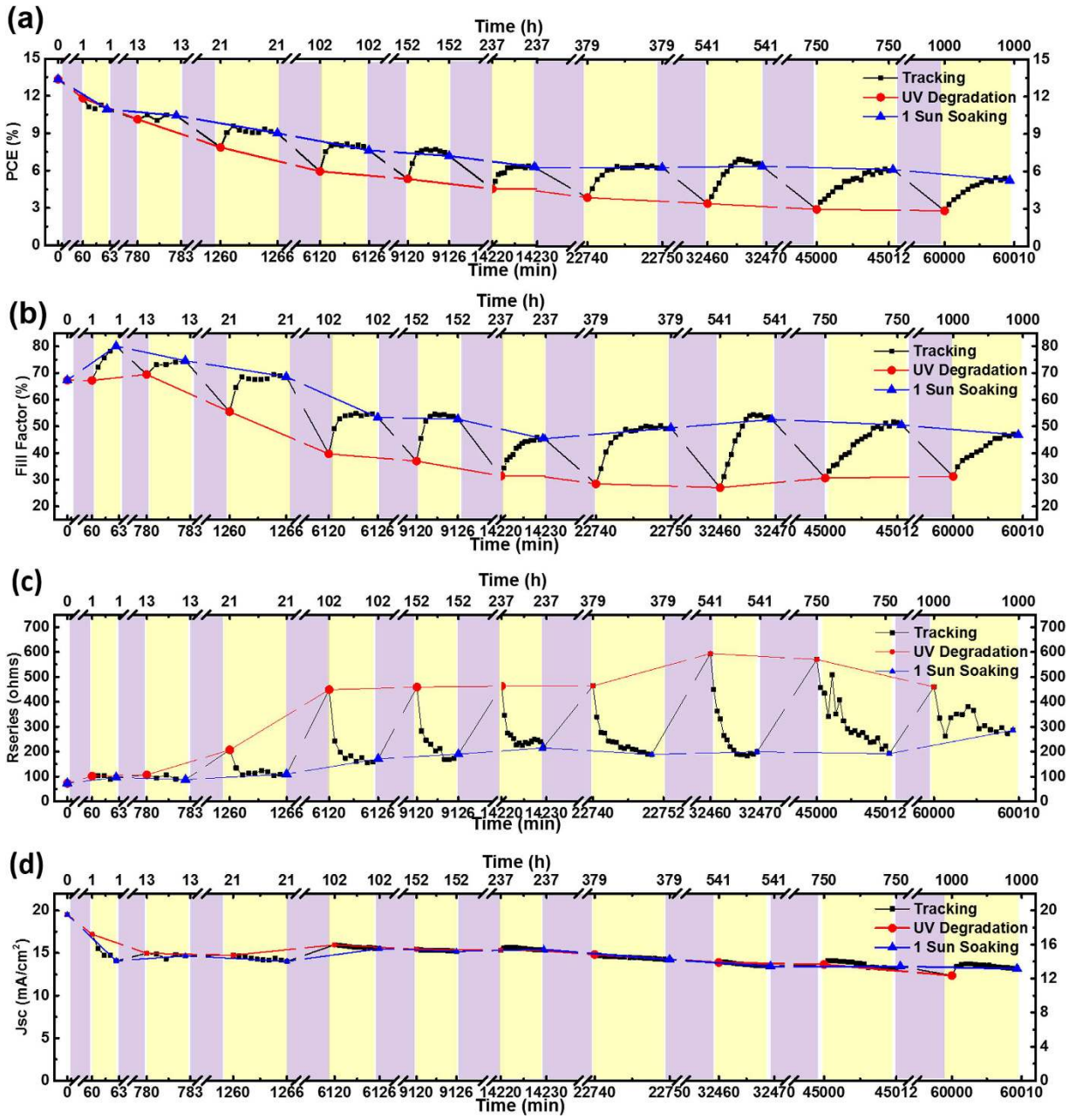

Figure 5. UV degradation/recovery cycle of (**a**) PCE, (**b**) FF, (**c**) R_s, and (**d**) J_{sc} for device subjected to a range of UV exposure and 1-sun light illumination. Purple regions represent UV exposure and yellow regions represent 1-sun light illumination periods. The breaks used in this figure. Red (circle) symbol denotes values after UV exposure and blue (triangle) symbol denotes values after 1-sun light illumination. Black (square) symbol denotes values during 1-sun light illumination. Lines between the symbols are guide to the eyes. V_{oc} data is shown in Supplementary Fig. S5. Data for other devices showing similar tendency are presented in Supplementary Figs S6–10.

Aldrich) in a 1.1:1 molar ratio. After spin-coating PbI_2 on the mesoporous TiO_2 film, annealing was carried out first at 40 °C for 3 min and then at 75 °C for 10 min. A dipping solution was prepared; the solution contained methylammonium iodide (MAI, 0.9 g, Dyesol) dispersed in isopropyl alcohol (IPA, 10 mL, anhydrous, 99.5%, Sigma Aldrich). The PbI_2 film was immersed in the solution prior to annealing at 100 °C for 30 min. 2,2′,7,7′-Tetrakis(*N*,*N*-di-*p*-methoxyphenyl-amine)-9,9′-spirobifluorene (Spiro-MeOTAD, HANALINTECH), doped with bis(trifluoromethane)sulfonimide lithium salt (Li-TSFI, 99.95% trace metals basis, Sigma-Aldrich) was used as an HTM. A solution of the HTM was prepared by dissolving Spiro-MeOTAD (72.3 mg) in chlorobenzene (1 mL, 99.8% Sigma-Aldrich) containing 4-tert-butyl pyridine (28.8 μL, 96%, Sigma-Aldrich) and Li-TSFI solution (17.5 μL,

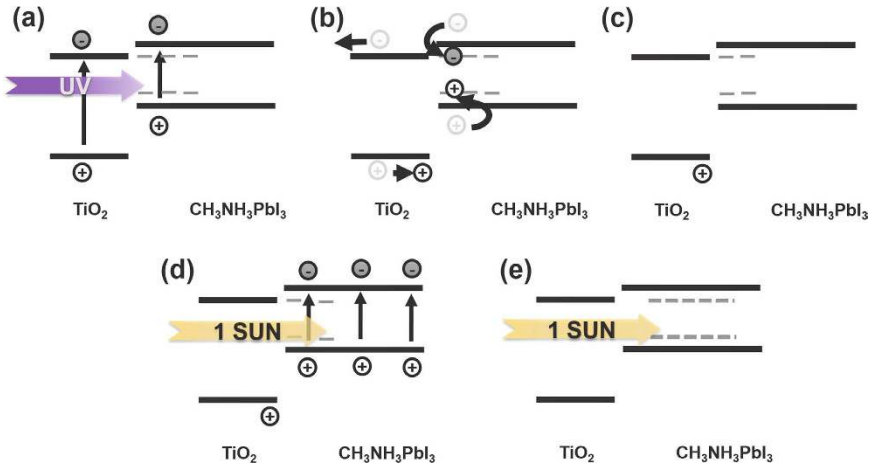

Figure 6. Schematic representation of the proposed mechanisms for UV degradation and recovery of perovskite solar cells.

520 mg Li-TSFI in 1 mL anhydrous acetonitrile (99.8%, Sigma-Aldrich)). Finally, a 100 nm Au electrode was deposited by thermal evaporation.

The UV degradation experiment was conducted in a glove box at 25 °C under an inert (Ar) atmosphere at <0.5 ppm humidity. Regeneration of the glove box atmosphere was performed twice to control the humidity and to remove traces of solvent. The perovskite solar cells were exposed to 4 W, 365 nm (VL-4.LC, VILBER LOURMAT, 350 $\mu W \cdot cm^{-2}$ at 15 cm) UV light for 1,000 h, 2 cm above the samples. UV light irradiation at 2 cm apart from UV lamp shows 19 Lux ($=7.6\,mW \cdot cm^{-2}$ in case of Sunlight), which was measured by Testo 540-Lux Meter.

1-Sun light illumination for the recovery experiment was performed under 100 $mW \cdot cm^{-2}$ irradiation at room temperature and 25% average relative humidity. The device temperature was approximately 40 °C after 10 min 1-sun light irradiation. All devices were illuminated with a 0.075 cm^2 mask.

Device characterization. The UV-induced degradation of the perovskite solar cells was studied over a range of time intervals. The cells were removed from the glove box at specifically defined times and characterized under air at room temperature and 25% average relative humidity.

The light absorbance and transmittance were measured by UV-Vis spectroscopy (JASCO V-670 UV/Vis NIR spectrophotometer), and X-ray diffractometry (XRD, SmartLab, Rigaku) was carried out using CuKα radiation (1.54 nm). The solar cell parameters of the devices were measured using a solar simulator (WXS-155S-10, AG1.5G, WACOM) under 100 $mW \cdot cm^{-2}$ irradiation. All devices had an active area of 0.125 cm^2 and all light I-V measurements were performed using a 0.075 cm^2 mask. The scan direction was open circuit voltage to short circuit current (i.e., reverse direction) and the voltage setting time was 200 ms. External quantum efficiency measurements were conducted using a 100 Hz chopping frequency.

Electrochemical Impedance spectroscopy measurements were performed with IVIUM, IviumStat by applying the alternative signal of 10 mV at ten points per decade in the frequency range of 10^6~1 Hz with DC voltage set point under dark conditions. The obtained Nyquist plots were modelled by using Z-View software.

The μ-PLS and μ-LBIC mappings were performed with a photoluminescence spectroscopy setup using a confocal microscope, illuminating the samples from the glass side[66,67]. The point-shaped excitation and detection allows for diffraction limited resolution when using an objective lens with a low numerical aperture (<0.1). In this case, an objective lens with a numerical aperture (NA) of 0.26 was used in order to enhance the detection spot size and therefore allow for a reduction of the integration time. For both measurements, an excitation wavelength of 640 nm and an illumination intensity of 3 μW, with a laser spot size of 430 μm^2, were chosen. For detection of the PL signal, a silicon line CCD combined with a grating spectrometer was used, providing the PL spectrum for each measurement spot. In order to suppress the excitation light, a 700 nm longpass filter was applied. Both the spectral position and the peak height were obtained from a Gaussian fit of the measurement data. As the local light beam-induced current is very low, the signal was amplified using a low noise preamplifier.

References

1. Kojima, A., Teshima, K., Shirai, Y. & Miyasaka, T. Organometal halide perovskites as visible-light sensitizers for photovoltaic cells. *J. Am. Chem. Soc.* **131,** 6050–6051, doi: 10.1021/ja809598r (2009).
2. NREL Efficiency Chart. http://www.nrel.gov/ncpv/images/ efficiency_chart.jpg (accessed June 29, 2016).
3. Green, M. A., Ho-Baillie, A. & Snaith, H. J. The emergence of perovskite solar cells. *Nat. Photonics* **8,** 506–514, doi: 10.1038/Nphoton.2014.134 (2014).
4. Snaith, H. J. Perovskites: the emergence of a new era for low-cost, high-efficiency solar cells. *J. Phys. Chem. Lett.* **4,** 3623–3630, doi: 10.1021/jz4020162 (2013).
5. Kim, H. S., Im, S. H. & Park, N. G. Organolead halide perovskite: new horizons in solar cell research. *J. Phys. Chem. C* **118,** 5615–5625, doi: 10.1021/jp409025w (2014).

6. Lee, J. W. *et al.* Formamidinium and cesium hybridization for photo- and moisture-stable perovskite solar cell. *Adv. Energy Mater.* **5,** doi: 1002/Aenm.201501310 (2015).
7. McMeekin, D. P. *et al.* A mixed-cation lead mixed-halide perovskite absorber for tandem solar cells. *Science* **351,** 151–155, doi: 10.1126/science.aad5845 (2016).
8. Eperon, G. E. *et al.* Inorganic caesium lead iodide perovskite solar cells. *J. Mater. Chem. A* **3,** 19688–19695, doi: 10.1039/c5ta06398a (2015).
9. De Marco, N. *et al.* Guanidinium: a route to enhanced carrier lifetime and open-circuit voltage in hybrid perovskite solar cells. *Nano Lett.* **16,** 1009–1016, doi: 10.1021/acs.nanolett.5b04060 (2016).
10. Kim, H. S. *et al.* Lead iodide perovskite sensitized all-solid-state submicron thin film mesoscopic solar cell with efficiency exceeding 9%. *Sci. Rep.* **2,** doi: 1038/Srep00591 (2012).
11. Chen, C. W. *et al.* Optical properties of organometal halide perovskite thin films and general device structure design rules for perovskite single and tandem solar cells. *J. Mater. Chem. A* **3,** 9152–9159, doi: 10.1039/c4ta05237d (2015).
12. Lin, Q. Q., Armin, A., Nagiri, R. C. R., Burn, P. L. & Meredith, P. Electro-optics of perovskite solar cells. *Nat. Photonics* **9,** 106–112, doi: 10.1038/Nphoton.2014.284 (2015).
13. Loper, P. *et al.* Complex refractive index spectra of CH3NH3PbI3 perovskite thin films determined by spectroscopic ellipsometry and spectrophotometry. *J. Phys. Chem. Lett.* **6,** 66–71, doi: 10.1021/jz502471h (2015).
14. Xie, Z. *et al.* Refractive index and extinction coefficient of CH3NH3PbI3 studied by spectroscopic ellipsometry. *Opt. Mater. Express* **5,** 29–43, doi: 10.1364/Ome.5.000029 (2015).
15. Wehrenfennig, C., Liu, M. Z., Snaith, H. J., Johnston, M. B. & Herz, L. M. Charge-carrier dynamics in vapour-deposited films of the organolead halide perovskite CH3NH3PbI3-xClx. *Energy Environ. Sci.* **7,** 2269–2275, doi: 10.1039/c4ee01358a (2014).
16. Gonzalez-Pedro, V. *et al.* General working principles of CH3NH3PbX3 perovskite solar cells. *Nano Lett.* **14,** 888–893, doi: 10.1021/nl404252e (2014).
17. Burschka, J. *et al.* Sequential deposition as a route to high-performance perovskite-sensitized solar cells. *Nature* **499,** 316-+, doi: 10.1038/nature12340 (2013).
18. Eperon, G. E., Burlakov, V. M., Docampo, P., Goriely, A. & Snaith, H. J. Morphological control for high performance, solution-processed planar heterojunction perovskite solar cells. *Adv. Funct. Mater.* **24,** 151–157, doi: 10.1002/adfm.201302090 (2014).
19. Liu, M. Z., Johnston, M. B. & Snaith, H. *J. Efficient planar heterojunction perovskite solar cells by vapour deposition. Nature* **501,** 395-+, doi: 10.1038/nature12509 (2013).
20. Malinkiewicz, O. *et al.* Perovskite solar cells employing organic charge-transport layers. *Nat. Photonics* **8,** 128–132, doi: 10.1038/Nphoton.2013.141 (2014).
21. Chen, Q. *et al.* Planar heterojunction perovskite solar cells via vapor-assisted solution process. *J. Am. Chem. Soc.* **136,** 622–625, doi: 10.1021/ja411509g (2014).
22. Hoke, E. T. *et al.* Reversible photo-induced trap formation in mixed-halide hybrid perovskites for photovoltaics. *Chem. Sci.* **6,** 613–617, doi: 10.1039/c4sc03141e (2015).
23. Noh, J. H., Im, S. H., Heo, J. H., Mandal, T. N. & Seok, S. I. Chemical management for colorful, efficient, and stable inorganic-organic hybrid nanostructured solar cells. *Nano Lett.* **13,** 1764–1769, doi: 10.1021/nl400349b (2013).
24. Mailoa, J. P. *et al.* A 2-terminal perovskite/silicon multijunction solar cell enabled by a silicon tunnel junction. *Appl. Phys. Lett.* **106,** doi: 1063/1.4914179 (2015).
25. Werner, J. *et al.* Efficient monolithic perovskite/silicon tandem solar cell with cell area >1 cm(2). J. *Phys. Chem. Lett.* **7,** 161–166, doi: 10.1021/acs.jpclett.5b02686 (2016).
26. Albrecht, S. *et al.* Monolithic perovskite/silicon-heterojunction tandem solar cells processed at low temperature. *Energy Environ. Sci.* **9,** 81–88, doi: 10.1039/c5ee02965a (2016).
27. Loper, P. *et al.* Organic-inorganic halide perovskite/crystalline silicon four-terminal tandem solar cells. *Phys. Chem. Chem. Phys.* **17,** 1619–1629, doi: 10.1039/c4cp03788j (2015).
28. Noel, N. K. *et al.* Lead-free organic-inorganic tin halide perovskites for photovoltaic applications. *Energy Environ. Sci.* **7,** 3061–3068, doi: 10.1039/c4ee01076k (2014).
29. Kumar, M. H. *et al.* Lead-free halide perovskite solar cells with high photocurrents realized through vacancy modulation. *Adv. Mater.* **26,** 7122-+, doi: 10.1002/adma.201401991 (2014).
30. Hao, F., Stoumpos, C. C., Cao, D. H., Chang, R. P. H. & Kanatzidis, M. G. Lead-free solid-state organic-inorganic halide perovskite solar cells. *Nat. Photonics* **8,** 489–494, doi: 10.1038/nphoton.2014.82 (2014).
31. Deng, Y. H. *et al.* Scalable fabrication of efficient organolead trihalide perovskite solar cells with doctor-bladed active layers. *Energy Environ. Sci.* **8,** 1544–1550, doi: 10.1039/c4ee03907f (2015).
32. Hwang, K. *et al.* Toward large scale roll-to-roll production of fully printed perovskite solar cells. *Adv. Mater.* **27,** 1241–1247, doi: 10.1002/adma.2014045 98 (2015).
33. Wei, Z. H., Chen, H. N., Yan, K. Y. & Yang, S. H. Inkjet printing and instant chemical transformation of a CH3NH3PbI+/ nanocarbon electrode and interface for planar perovskite solar cells. *Angew. Chem., Int. Ed.* **53,** 13239–13243, doi: 10.1002/anie.201408638 (2014).
34. Niu, G. D. *et al.* Study on the stability of CH3NH3PbI3 films and the effect of post-modification by aluminum oxide in all-solid-state hybrid solar cells. *J. Mater. Chem. A* **2,** 705–710, doi: 10.1039/c3ta13606j (2014).
35. Niu, G. D., Guo, X. D. & Wang, L. D. Review of recent progress in chemical stability of perovskite solar cells. *J. Mater. Chem. A* **3,** 8970–8980, doi: 10.1039/c4ta04994b (2015).
36. Yang, J. L., Siempelkamp, B. D., Liu, D. Y. & Kelly, T. L. Investigation of CH3NH3PbI3 degradation rates and mechanisms in controlled humidity environments using *in situ* techniques. *ACS Nano* **9,** 1955–1963, doi: 10.1021/nn506864k (2015).
37. Habisreutinger, S. N. *et al.* Carbon nanotube/polymer composites as a highly stable hole collection layer in perovskite solar cells. *Nano Lett.* **14,** 5561–5568, doi: 10.1021/nl501982b (2014).
38. Li, X. *et al.* Improved performance and stability of perovskite solar cells by crystal crosslinking with alkylphosphonic acid omega-ammonium chlorides. *Nat. Chem.* **7,** 703–711, doi: 10.1038/Nchem.2324 (2015).
39. Xiao, Z. G. *et al.* Giant switchable photovoltaic effect in organometal trihalide perovskite devices. *Nat. Mater.* **14,** 193–198, doi: 10.1038/NMAT4150 (2015).
40. Leijtens, T. *et al.* Overcoming ultraviolet light instability of sensitized TiO2 with meso-superstructured organometal tri-halide perovskite solar cells. *Nat. Commun.* **4,** doi: 1038/Ncomms3885 (2013).
41. Han, Y. *et al.* Degradation observations of encapsulated planar CH3NH3PbI3 perovskite solar cells at high temperatures and humidity. *J. Mater. Chem. A* **3,** 8139–8147, doi: 10.1039/c5ta00358j (2015).
42. Mei, A. Y. *et al.* A hole-conductor-free, fully printable mesoscopic perovskite solar cell with high stability. *Science* **345,** 295–298, doi: 10.1126/science.1254763 (2014).
43. Hu, M. *et al.* Efficient hole-conductor-free, fully printable mesoscopic perovskite solar cells with a broad light harvester NH2CH = NH(2)PbI(3). *J. Mater. Chem. A* **2,** 17115–17121, doi: 10.1039/c4ta03741c (2014).
44. Li, W. Z. *et al.* Enhanced UV-light stability of planar heterojunction perovskite solar cells with caesium bromide interface modification. *Energy Environ. Sci.* **9,** 490–498, doi: 10.1039/c5ee03522h (2016).
45. Ito, S., Tanaka, S., Manabe, K. & Nishino, H. Effects of surface blocking layer of Sb2S3 on nanocrystalline TiO2 for CH3NH3PbI3 perovskite solar cells. *J. Phys. Chem. C* **118,** 16995–17000, doi: 10.1021/jp500449z (2014).

46. Heo, J. H., Han, H. J., Kim, D., Ahn, T. K. & Im, S. H. Hysteresis-less inverted CH3NH3PbI3 planar perovskite hybrid solar cells with 18.1% power conversion efficiency. *Energy Environ. Sci.* **8,** 1602–1608, doi: 10.1039/c5ee00120j (2015).
47. Hinsch, A. *et al.* Introduction to *in-situ* produced perovskite solar cells; a new concept towards lowest module manufacturing costs. Presented at the 29th European PV Solar Energy Conference and Exhibition, 22–26 September 2014, Amsterdam, The Netherlands.
48. Murugadoss, G. *et al.* Light stability tests of methylammonium and formamidinium Pb-halide perovskites for solar cell applications. *Jpn. J. Appl. Phys.* **54,** doi: 10.7567/Jjap.54.08kf08 (2015).
49. Li, X. *et al.* Outdoor performance and stability under elevated temperatures and long-term light soaking of triple-layer mesoporous perovskite photovoltaics. *Energy Technol-Ger.* **3,** 551–555, doi: 10.1002/ente.201500045 (2015).
50. Kwon, Y. S., Lim, J., Yun, H. J., Kim, Y. H. & Park, T. A diketopyrrolopyrrole-containing hole transporting conjugated polymer for use in efficient stable organic-inorganic hybrid solar cells based on a perovskite. *Energy Environ. Sci.* **7,** 1454–1460, doi: 10.1039/c3ee44174a (2014).
51. Cao, D. Y. H. *et al.* Remnant PbI2, an unforeseen necessity in high-efficiency hybrid perovskite-based solar cells? *Appl. Mater.* **2,** doi: 1063/14895038 (2014).
52. Chen, Q. *et al.* Controllable self-induced passivation of hybrid lead iodide perovskites toward high performance solar cells. *Nano Lett.* **14,** 4158–4163, doi: 10.1021/nl501838y (2014).
53. Kim, Y. C. *et al.* Beneficial effects of PbI2 incorporated in organo-lead halide perovskite solar cells. *Adv. Energy Mater.* **6,** doi: 1002/Aenm.201502104 (2016).
54. Supasai, T., Rujisamphan, N., Ullrich, K., Chemseddine, A. & Dittrich, T. Formation of a passivating CH3NH3PbI3/PbI2 interface during moderate heating of CH3NH3PbI3 layers. *Appl. Phys. Lett.* **103,** doi: 10.1063/1.4826116 (2013).
55. Liu, F. *et al.* Is excess PbI2 beneficial for perovskite solar cell performance? *Adv. Energy Mater.* **6,** doi: 10.1002/aenm.201502206 (2016).
56. Zhao, Ying *et al.* "Improving the efficiency of perovskite solar cells through optimization of the CH 3 NH 3 PbI 3 film growth in solution process method."*Applied Surface Science* **359,** 560–566 (2015).
57. Zhao, C. *et al.* Revealing underlying processes involved in light soaking effects and hysteresis phenomena in perovskite solar cells. *Adv. Energy Mater.* **5,** doi: 1002/Aenm.201500279 (2015).
58. Snaith, H. J. *et al.* Anomalous hysteresis in perovskite solar cells. *J. Phys. Chem. Lett.* **5,** 1511–1515, doi: 10.1021/jz500113x (2014).
59. Docampo, P., Ball, J. M., Darwich, M., Eperon, G. E. & Snaith, H. J. Efficient organometal trihalide perovskite planar-heterojunction solar cells on flexible polymer substrates. *Nat. Commun.* **4,** doi: 1038/Ncomms3761 (2013).
60. Small, C. E. *et al.* High-efficiency inverted dithienogermole-thienopyrrolodione-based polymer solar cells. *Nat. Photonics* **6,** 115–120 (2012).
61. Unger, E. L. *et al.* Hysteresis and transient behavior in current-voltage measurements of hybrid-perovskite absorber solar cells. *Energy Environ. Sci.* **7,** 3690–3698, doi: 10.1039/c4ee02465f (2014).
62. Nie, W. *et al.* Light-activated photocurrent degradation and self-healing in perovskite solar cells. *Nat. Commun.* **7,** doi: 1038/Ncomms11574 (2016).
63. Neukirch, A. J. *et al.* Polaron stabilization by cooperative lattice distortion and cation rotations in hybrid perovskite materials. *Nano Lett*, **16,** 3809–3816, doi: 10.1021/acs.nanolett.6b01218 (2016).
64. Gottesman, R. & Zaban, A. Perovskites for photovoltaics in the spotlight: photoinduced physical changes and their implications. *Acc. Chem. Res.* **49,** 320–329, doi: 10.1021/acs.accounts.5b00446 (2016).
65. Kim, H. S. *et al.* Mechanism of carrier accumulation in perovskite thin-absorber solar cells. *Nat Commun* **4,** doi: 10.1038/Ncomms3242 (2013).
66. Gundel, P., Heinz, F. D., Schubert, M. C., Giesecke, J. A. & Warta, W. Quantitative carrier lifetime measurement with micron resolution. *J. Appl. Phys.* **108,** doi: 1063/1.3462433 (2010).
67. Mastroianni, S. *et al.* Analysing the effect of crystal size and structure in highly efficient $CH_3NH_3PbI_3$ perovskite solar cells by spatially resolved photo- and electroluminescence imaging. *Nanoscale* **7,** 19653–19662 doi: 10.1039/c5nr05308k (2015).

Acknowledgements

This work was supported by a grant (No. 20138520011170) from the financial resources of the Ministry of Trade, Industry & Energy, Republic of Korea. This work was also supported by the National Research Foundation of Korea Grant funded by the Korean Government(MSIP) (2016, University-Institute cooperation program).

Author Contributions

S.-W.L. contributed to the overall project. S.K. and S.B. performed the data analysis. T.C. and K.C. fabricated the perovskite solar cell and performed several measurements. L.E.M. wrote a part of the manuscript and performed μ-PLS and μ-LBIC measurement and analysis. Y.K. and Y.J. conducted EIS measurement and analysis. S.L., S.P., H.P., M.C.S., S.G., Y.K., H.-S.L., and D.K. directed the project. All authors reviewed the manuscript.

Additional Information

Supplementary information accompanies this paper at http://www.nature.com/srep

Competing financial interests: The authors declare no competing financial interests.

How to cite this article: Lee, S.-W. *et al.* UV Degradation and Recovery of Perovskite Solar Cells. *Sci. Rep.* **6**, 38150; doi: 10.1038/srep38150 (2016).

Publisher's note: Springer Nature remains neutral with regard to jurisdictional claims in published maps and institutional affiliations.

This work is licensed under a Creative Commons Attribution 4.0 International License. The images or other third party material in this article are included in the article's Creative Commons license, unless indicated otherwise in the credit line; if the material is not included under the Creative Commons license, users will need to obtain permission from the license holder to reproduce the material. To view a copy of this license, visit http://creativecommons.org/licenses/by/4.0/

© The Author(s) 2016